Microscopic cluster model analysis of $^{14}O + p$ elastic scattering

D. Baye,[1,2,*] P. Descouvemont,[2,†] and F. Leo[1]
[1]*Physique Quantique, C.P. 165/82, Université Libre de Bruxelles, B-1050 Brussels, Belgium*
[2]*Physique Nucléaire Théorique et Physique Mathématique, C.P. 229, Université Libre de Bruxelles, B-1050 Brussels, Belgium*
(Received 25 April 2005; published 16 August 2005)

The $^{14}O + p$ elastic scattering is discussed in detail in a fully microscopic cluster model. The ^{14}O cluster is described by a closed p shell for protons and a closed $p3/2$ subshell for neutrons in the translation-invariant harmonic-oscillator model. The exchange and spin-orbit parameters of the effective forces are tuned on the energy levels of the ^{15}C mirror system. With the generator-coordinate and microscopic R-matrix methods, phase shifts and cross sections are calculated for the $^{14}O + p$ elastic scattering. An excellent agreement is found with recent experimental data. A comparison is performed with phenomenological R-matrix fits. Resonances properties in ^{15}F are discussed.

DOI: 10.1103/PhysRevC.72.024309 PACS number(s): 25.40.Cm, 21.60.Gx, 24.10.Cn, 27.20.+n

I. INTRODUCTION

Unbound nuclei just beyond the proton drip line can now be studied experimentally with scattering experiments involving short-lived radioactive ion beams. In particular, recent studies have focused on the spectrum of ^{15}F in relation with the possible disappearance of the $Z = 8$ magic number [1,2]. This unbound nucleus is studied with the $^{14}O + p$ elastic scattering in reversed kinematics with low-energy beams. The measured cross sections provide information about the low-lying resonance spectrum of ^{15}F but their analysis relies on different simplifying assumptions which should be assessed by more elaborate models.

The aim of the present paper is to perform an analysis of the $^{14}O + p$ elastic scattering within the resonating group method (RGM). The RGM gives fair results for a similar collision, the $^{16}O + p$ elastic scattering [3]. In this microscopic model, the wave functions of the system are derived from shell-model internal wave functions of the individual clusters. Once the effective interaction and cluster descriptions are selected, this model does not depend on any parameter. In microscopic cluster models, antisymmetrization is exactly taken into account and the whole information is deduced from an effective nuclear force [4–7]. Standard effective interactions often depend on some exchange parameter [8,9]. In the present case, such parameters can be tuned on the bound-state energies of the mirror ^{15}C nucleus described as a $^{14}C + n$ system. The only remaining choice is then the ^{14}O or ^{14}C cluster description. The ^{14}O cluster is described by a closed p shell for protons and a closed $p3/2$ subshell for neutrons in the translation-invariant harmonic oscillator model. The mirror structure is used for the ^{14}C cluster. The cluster assumption is expected to be well valid here since ^{14}O and ^{14}C have high inelastic excitation energies.

In the following, we present a fully microscopic study of the $^{14}O + p$ elastic scattering, performed with two effective nucleon-nucleon forces [8,9]. A comparison of the microscopic results with experimental excitation functions [1,2] allows us to discuss different properties of the resonances in the ^{15}F spectrum. We also take advantage of this calculation to perform phenomenological R-matrix fits [10] and to compare them with the microscopic analysis.

In Sec. II, the microscopic model is summarized. In Sec. III, elastic cross sections are calculated with the RGM. Phenomenological R-matrix fits are performed and discussed in Sec. IV. Concluding remarks are presented in Sec. V.

II. MICROSCOPIC MODEL

The system is described by an A-body microscopic Hamiltonian

$$H = \sum_{i=1}^{A} T_i + \sum_{i>j=1}^{A} V_{ij}, \tag{1}$$

with $A = 15$. In this Hamiltonian, T_i is the kinetic energy of nucleon i and V_{ij} is an effective interaction (including Coulomb and spin-orbit terms) between nucleons i and j. The same type of Hamiltonian with $A = 14$ is used to calculate the cluster energies.

The colliding nuclei have spins 0 and 1/2 leading to a channel spin $I = 1/2$. The orbital momentum l coupled to the channel spin I gives the total angular momentum J, and the parity $(-1)^l$. For partial wave lJ, the bound and scattering wave functions of the system are described by resonating-group wave functions [4,6] as

$$\Psi_l^{JM} = \mathcal{A}\phi_O[\phi_p \otimes Y_l(\Omega_\rho)]^{JM} u_l^J(\rho)/\rho, \tag{2}$$

where ϕ_O is the internal wave function chosen for describing the ^{14}O cluster, ϕ_p is the spin-isospin state of the proton, and $\boldsymbol{\rho} = (\rho, \Omega_\rho)$ is the quantal relative coordinate between the proton and the center of mass of the cluster. A similar definition holds for the $^{14}C + n$ mirror system. In Eq. (2), $u_l^J(\rho)$ is the relative wave function, and the operator $\mathcal{A}$ represents the antisymmetrizor over A nucleons.

*Electronic address: dbaye@ulb.ac.be
†Electronic address: pdesc@ulb.ac.be

The asymptotic form of a scattering-state relative wave function can be written as

$$u_l^J(\rho) \underset{\rho\to\infty}{\longrightarrow} \cos\delta_l^J F_l(k\rho) + \sin\delta_l^J G_l(k\rho), \tag{3}$$

where F_l and G_l are the regular and irregular Coulomb functions [11]. In Eq. (3), k is the wave number of the relative motion and δ_l^J is the scattering phase shift.

A direct use of the resonating-group wave functions (2) is not easy. An important simplification is obtained with the introduction of generator coordinates [5–7]. A Slater determinant in the two-center harmonic-oscillator model is defined as

$$\Phi_K(\boldsymbol{R}) = \mathcal{A}\Phi_O\left(-\tfrac{1}{15}\boldsymbol{R}\right)\Phi_{pK}\left(\tfrac{14}{15}\boldsymbol{R}\right). \tag{4}$$

In this expression $\Phi_O(\boldsymbol{S})$ is a Slater determinant defined in the harmonic oscillator model centered at $\boldsymbol{S}$ and $\Phi_{pK}(\boldsymbol{S})$ represents a $0s$ orbital (with spin and isospin) in the same model. The subscript $K = \pm 1/2$ corresponds to the proton spin projections. The ^{14}O cluster is described in the jj coupling scheme by a closed p shell for protons and a closed $p3/2$ subshell for neutrons.

The translation-invariant internal wave functions ϕ_O and ϕ_p appearing in Eq. (2) differ from $\Phi_O(\boldsymbol{S})$ and $\Phi_p(\boldsymbol{S})$ by a Gaussian center-of-mass (c.m.) factor centered at $\boldsymbol{S}$. The vector $\boldsymbol{R}$ joining the oscillator centers is the generator coordinate. A common oscillator parameter b is used on both centers. With this choice and the locations of the clusters employed in Eq. (4), the total c.m. motion factorizes as a simple $0s$ harmonic-oscillator orbital centered at the origin.

The Slater determinant (4) is then projected on the orbital and total angular momenta as [12]

$$\Phi_l^{JM}(R) = \frac{1}{4\pi}\sum_K (lIM-KK|JM)\int Y_l^{M-K} \times(\Omega_R)\Phi_K(\boldsymbol{R})d\Omega_R, \tag{5}$$

where $\boldsymbol{R} = (R, \Omega_R)$. The bound and scattering wave functions are expanded as

$$\Psi_l^{JM} \approx \sum_{n=1}^{N} f_{ln}^J \Phi_l^{JM}(R_n), \tag{6}$$

where N is the number of selected values for the generator coordinate R. The generator-coordinate values R_n are usually chosen equidistant. Expression (6) is equivalent to Eq. (2) except for the $0s$ Gaussian c.m. factor whose effect can be eliminated exactly and easily [7,13]. The relative function $u_l^J(r)$ depends on the coefficients f_{ln}^J which must be derived from the Hamiltonian H.

The expression (6) for the mirror system provides fair approximations of the ^{15}C bound states described with ^{14}C and neutron clusters. However these equations do not provide correct asymptotic properties for scattering states whose oscillating asymptotic behavior (3) cannot be simulated by a finite number of square-integrable functions. Expression (6) will therefore only be used in a limited range of ρ values and the correct asymptotic forms (2) and (3) will be obtained with the help of the microscopic R-matrix method [14].

In the microscopic R-matrix formalism [7,13,14], the configuration space is divided into two regions, separated at a distance a, the channel radius. In the internal region ($\rho < a$), the internal wave function $\Psi_{l,\mathrm{int}}^{JM}$ is described by approximation (6) in the microscopic cluster model with full account of antisymmetrization. In the external region ($\rho > a$), the antisymmetrization and the nuclear interaction between the cluster nucleons and the external nucleon are neglected. The external wave function

$$\Psi_{l,\mathrm{ext}}^{JM} \approx \phi_O[\phi_p \otimes Y_l(\Omega_\rho)]^{JM} \times\left[\cos\delta_l^J F_l(k\rho) + \sin\delta_l^J G_l(k\rho)\right]/\rho \tag{7}$$

involves a relative wave function u_l^J replaced by its exact asymptotic form (3). The validity of Eq. (7) implies a rather large value for the channel radius a. If a is large enough, the results must be independent of its value.

The microscopic R-matrix method provides a theoretical R matrix

$$R_l^J(E) = \sum_{\nu=0}^{N-1}\frac{\gamma_{lJ\nu}^2}{E_{lJ\nu}-E}, \tag{8}$$

where $\gamma_{lJ\nu}$ is the reduced width amplitude associated with pole $E_{lJ\nu}$. These quantities are obtained from matrix elements of the overlap, kinetic energy, central nuclear, spin-orbit, and Coulomb interactions between projected Slater determinants (5) according to a standard procedure [7,12,13]. The number of terms in Eq. (8) is equal to the basis size. Contrary to the phenomenological R-matrix employed in fits of experimental data, this theoretical R matrix is completely determined by the Schrödinger equation with Hamiltonian (1) and does not rely on experiment.

In single-channel calculations, the phase shift δ_l^J is deduced from R_l^J with the relationships

$$\delta_l^J = \delta_{l,\mathrm{HS}}^J + \delta_{l,\mathrm{R}}^J, \tag{9}$$

where the hard-sphere and R-matrix phase shift are defined, respectively, as

$$\delta_{l,\mathrm{HS}}^J(E) = -\arctan\frac{F_l(ka)}{G_l(ka)},$$
$$\delta_{l,\mathrm{R}}^J(E) = \arctan\frac{P_l(E)R_l^J(E)}{1-S_l(E)R_l^J(E)}. \tag{10}$$

In these expressions, P_l and S_l are the penetration and shift functions, respectively [15]. Although the hard-sphere and R-matrix phase shifts do depend individually on the value of the channel radius a, the total phase shift (9) should not depend on a if the accuracy of the calculation (i.e., the number of basis states) is sufficient.

III. PHASE SHIFTS AND CROSS SECTIONS

The ^{14}O nucleus is described with the oscillator parameter $b = 1.6$ fm. A number $N = 10$ of generator coordinates have been selected from 0.9 to 9 fm with a step of 0.9 fm. The channel radius a is taken as 8.1 fm, a value for which the

TABLE I. Potential parameters m of the Volkov force [8] or u of the Minnesota force [9] and S_0 of the spin-orbit interaction [12] (in MeV fm^5) fitting the ^{15}C bound-state energies.

Potential	m or u	S_0
V2	0.5864	25.2
MN	0.9290	35.2

residual nuclear interaction between the proton and the cluster is negligible.

Two effective nucleon-nucleon interactions are employed: Volkov V2 (Ref. [8]) and Minnesota (hereafter referred to as MN, Ref. [9]). Their exchange parameter M or u and their spin-orbit amplitude S_0 [12] are slightly adjusted (see Table I) to reproduce the ^{15}C bound spectrum, i.e., the energies of the $1/2^+$ and $5/2^+$ states, respectively, located at -1.219 and -0.473MeV below threshold.

The $^{14}\mathrm{O} + p$ elastic phase shifts obtained with both interactions below 4 MeV are displayed in Fig. 1. Both $1/2^+$ and $5/2^+$ curves confirm the existence of a resonance. The other phase shifts are rather small, the largest one being $3/2^+$ which does not exceed a few degrees in this energy range. Since the exchange parameters of the effective interactions are adjusted with the ^{15}C mirror system, the ^{15}F resonances are not necessarily located at the exact experimental energies. We shall discuss these locations after a comparison with experiment.

Elastic excitation functions obtained with both interactions at different c.m. angles are presented in Fig. 2 where they are compared with data of Ref. [2]. They are obtained with phase shifts up to $J = 7/2$. The phase shifts are given by the sum of nuclear [R matrix and hard sphere, see Eq. (9)], and Coulomb contributions. Both experiments [1,2] have studied the extreme c.m. angle 180° but the cross section normalization in not given in Ref. [1]. In Ref. [2], additional excitation functions are presented but with slightly varying angles. Hence, for $\theta < 180°$, we perform every time two different calculations,

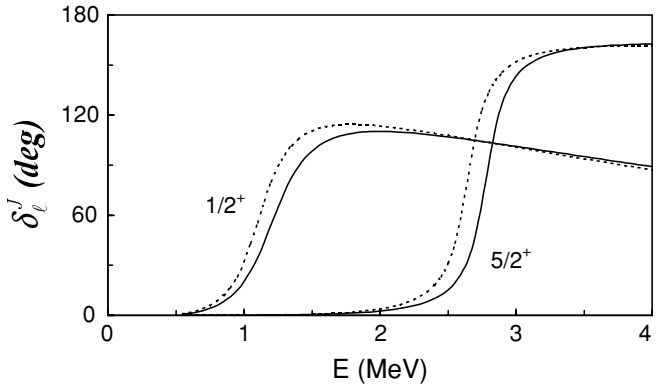

FIG. 1. Phase shifts δ_l^J for the $^{14}\mathrm{O} + p$ elastic scattering as a function of the c.m. energy E for the $1/2^+$ and $5/2^+$ partial waves calculated with the MN (solid lines) and V2 (dotted lines) forces.

one with the smallest angle of the covered energy range and one with the largest one. Agreement should be expected around the lower resonance for the lower angle and around the higher resonance for the higher angle. One observes that the curves obtained with V2 underestimate the energy locations of the resonance. The parameter M could be tuned to reproduce the experimental energies but charge symmetry of the nucleon-nucleon interaction would be broken. On the other hand, the cross sections obtained with MN reproduce fairly well both the resonance locations and their widths. This may be due to the fact that the MN force reproduces more correctly the low-energy nucleon-nucleon properties. The different experimental excitation functions progressively switch from the lower-angle cluster-model excitation function near 1 MeV to the higher-angle theoretical curve near 3 MeV. The agreement remains good even for the pair of smallest angles 106° and 124° While both resonances are quite well reproduced at all angles, the structures in the data between the resonances cannot be explained and may correspond to

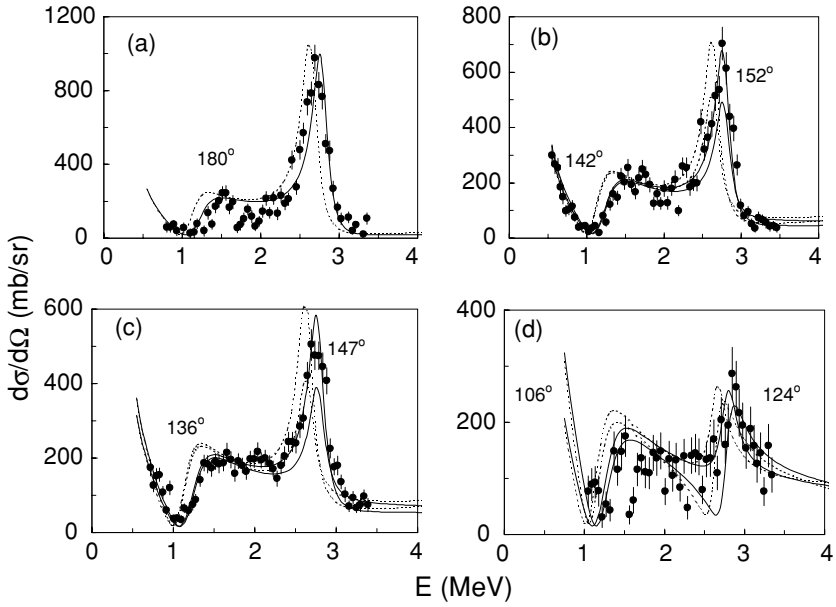

FIG. 2. Excitation functions for the $^{14}\mathrm{O} + p$ elastic scattering as a function of the c.m. energy E at c.m. angles of 180° (a), 142° and 152° (b), 136° and 147° (c), 106° and 124° (d), calculated with the MN (solid lines) and V2 (dotted lines) forces. Experimental cross sections from Ref. [2] correspond to a varying angle for $\theta < 180°$.

TABLE II. Microscopic R matrix results for $^{14}\mathrm{O}+p$ elastic scattering with the MN force [9]: first pole energy E_{lJ0}, reduced width γ^2_{lJ0}, resonance energy E_R, and width Γ_R (in MeV) at $a = 8.1$ fm. Experimental data are from Ref. [2].

	RGM				Exp.	
lJ	E_{lJ0}	γ^2_{lJ0}	E_R	Γ_R	E_R	Γ_R
$s1/2$	1.089	0.440	1.33	0.62	$1.29^{+0.08}_{-0.06}$, $1.45^{+0.16}_{-0.1}$	0.7
$d5/2$	2.615	0.137	2.79	0.23	2.795 ± 0.045	0.325 ± 0.06

statistical fluctuations. From now on, we only consider the MN force.

The microscopic R matrix parameters describing the resonances are given in Table II. The resonance parameters E_R and Γ_R are obtained with an iteration technique [16]. Their determination is illustrated in Fig. 3 for the $1/2^+$ resonance. According to Eq. (10), the resonance energy E_R and width Γ_R are defined by

$$1 - S_l(E_R)R_l^J(E_R) = 0,$$
$$\Gamma_R = \frac{2P_l(E_R)R_l^J(E_R)}{[S_l(E)R_l^J(E)]'_{E=E_R}}. \tag{11}$$

The energy E_R corresponds to the crossing between the curves representing the R matrix and the inverse of the s-wave shift function S_0 [15]. In the same figure is shown the background term R_0 of the R matrix defined by

$$R_l^J(E) = \frac{\gamma^2_{lJ0}}{E_{lJ0} - E} + R^J_{l0}(E), \tag{12}$$

i.e., the part of the R matrix remaining after removing the resonance. It is not negligible but does not depend much on energy. In phenomenological approaches, $R^J_{l0}(E)$ is usually set to zero.

The microscopic resonance energies can be compared with the experimental results. The $1/2^+$ ground-state energy is $E_R = 1.51 \pm 0.15$ MeV with a width $\Gamma_R = 1.2$ MeV in Ref. [1] and $E_R = 1.29^{+0.08}_{-0.06}$ MeV with a width $\Gamma_R = 0.7$ MeV or $E_R = 1.45^{+0.16}_{-0.10}$ MeV in Ref. [2] according to the technique of calculation. However, we will see in the next section that different $1/2^+$ properties may be deduced from the same data with R-matrix fits. The microscopic value $E_R = 1.33$ MeV seems to favor the lower experimental energy. The width $\Gamma_R = 0.62$ MeV is also somewhat smaller. We discuss the validity of the microscopic calculation in the next section.

For the narrower $5/2^+$ resonance, the experimental values are $E_R = 2.853 \pm 0.045$ MeV with $\Gamma_R = 0.34$ MeV [1] and $E_R = 2.795 \pm 0.045$ MeV with $\Gamma_R = 0.325 \pm 0.06$ MeV [2]. The microscopic energy $E_R = 2.79$ MeV is in excellent agreement with these values. The theoretical width $\Gamma_R = 0.23$ MeV is smaller. One observes indeed in Fig. 2 that the RGM does not reproduce well the lower-energy wing of the resonance. However, this is not true at 147° and 152°.

The role of the background term R_0 is analyzed in Figs. 4 and 5. In Fig. 4, the resonant $1/2^+$ phase shift obtained when neglecting R_0 is shown to deviate significantly from the microscopic result. On the other hand, with the energy-independent approximation $R_0 = 0.28$, the agreement becomes much better on resonance. In Fig. 5, excitation functions at 180° are calculated by replacing the $1/2^+$ and/or $5/2^+$ microscopic phase shifts by a single-pole approximation (12) with $R_0 = 0$. None of these approximations is able to reproduce the behavior of the microscopic cross section. Why is this possible in phenomenological analyses?

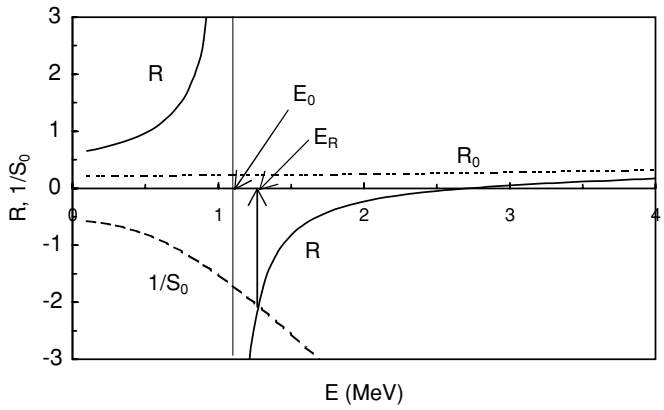

FIG. 3. Determination of the $1/2^+$ resonance energy $E_R \approx 1.33$ MeV: R matrix (solid line) and $1/S_0$ (dashed line). The background R_0 [Eq. (12)] is displayed as a dotted line. The pole energy E_0 and the resonance energy E_R and indicated by arrows.

IV. PHENOMENOLOGICAL *R*-MATRIX ANALYSIS

Let us emphasize that we make use in this paper of two different aspects of R-matrix theory. In nuclear physics, R-matrix theory [15] is often only considered as a powerful

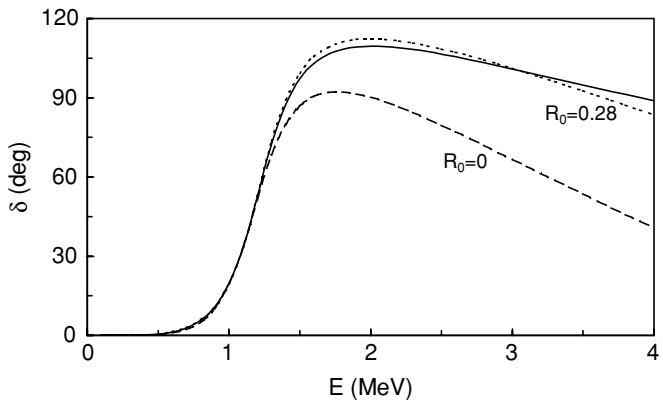

FIG. 4. Single-pole approximations of the microscopic $1/2^+$ phase shift (solid line): $R_0 = 0$ (dashed line) and $R_0 = 0.28$ (dotted line).

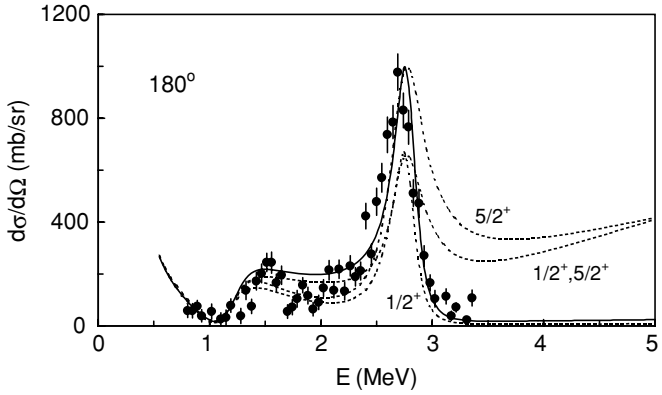

FIG. 5. Single-pole approximations (dotted lines) of the microscopic cross section at 180° (solid line). For the partial waves indicated on the curves, the RGM phase shifts are replaced by their approximation with $R_0 = 0$. Experimental cross sections are from Ref. [2].

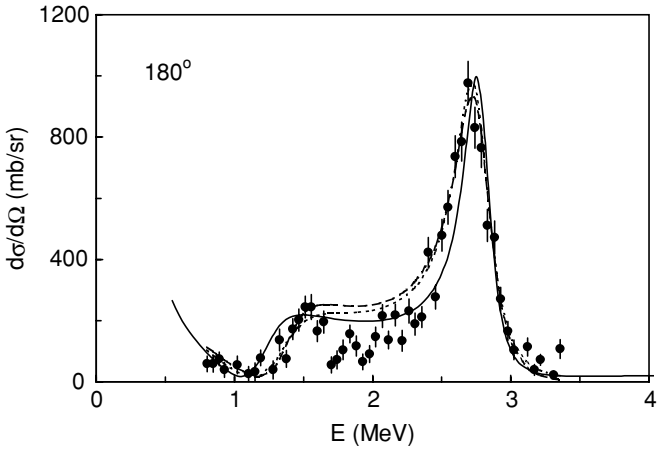

FIG. 6. Excitation functions for the ^{14}O + p elastic scattering at 180° calculated with the MN interaction (solid line) and with phenomenological R-matrix fits for $a = 4$ (dotted line) and 5 fm (dashed line). Experimental cross sections are from Ref. [2].

technique to fit data. This well-known aspect is here named phenomenological R matrix. However the R matrix is also a powerful tool to solve the Schrödinger equation, especially in the continuum [17,18]. This is for example the case with the microscopic R-matrix method [7,14] employed above.

Although the principles of these two aspects of R-matrix theory are common, an important difference concerns the choice of the channel radius a. When R-matrix theory is used to solve the Schrödinger equation, the value of a is irrelevant provided that it is large enough. In practice, one tries to keep it as small as allowed by the conditions that antisymmetrization and nuclear interaction be negligible in the external region in order to reduce the number of basis states. In the phenomenological R matrix, a is a parameter of the fit for which an optimal value should exist. This difference occurs because one tries to fit data with a very small number of terms in the R matrix. Hence some values are more efficient because they minimize the remaining background.

In order to analyze the resonance properties with different models, we now fit the data at 180° from Ref. [2] with only the $1/2^+$ and $5/2^+$ waves using single-pole phenomenological R matrices without background term for parametrizing both phase shifts. The other excitation functions correspond to unknown angles and would be difficult to use. The technique is similar to the one used in ^{7}Be + p scattering [10]. The results are displayed in Fig. 6. The obtained parameters and the energy and width of the resonances are given in Table III. In order to have good fits, the channel radius must be chosen around 5 fm, i.e., much smaller than in the microscopic model (8.1 fm). With that value, the results of the microscopic model would be meaningless. Numerically, the χ^2 values are equivalent for $a = 4$ fm and $a = 5$ fm and the resonance energies are similar, but the parameters obtained with $a = 4$ fm are unphysical. In that case, the reduced width is close or above the Wigner limit ($\gamma_W^2 = 4.16$ MeV).

TABLE III. Single-pole phenomenological R matrix fits of ^{14}O + p elastic scattering cross sections at 180° [2]: pole energy E_{lJ0}, reduced width γ_{lJ0}^2, resonance energy E_R, and width Γ_R (in MeV).

lJ	a	E_{lJ0}	γ_{lJ0}^2	E_R	Γ_R
$s1/2$	4	−0.59	3.57	1.50	0.84
	5	0.94	0.96	1.47	0.56
$d5/2$	4	−6.29	4.91	2.78	0.33
	5	−0.34	0.85	2.79	0.34

The $1/2^+$ resonance location is around 1.47 MeV, i.e., more than 0.1 MeV higher than with the RGM. The location of a rather broad resonance may significantly depend on model assumptions. In Fig. 6, one observes that the vicinity of the $1/2^+$ resonance is less well reproduced by the microscopic model. The resonance location is thus probably closer to the result of Table III. The phenomenological $1/2^+$ width depends on a. The width is probably smaller than suggested in Refs. [1,2].

The $5/2^+$ resonance energy is in good agreement with the RGM result. The microscopic width is significantly smaller. The pole locations and reduced widths are of course completely different from Table II. Figure 6 indeed shows that the RGM resonance is narrower than with the fits. The RGM result does not agree well with the left wing of the resonance but it agrees better with experiment between resonances. Also it correctly reproduces the resonance at other angles. The resonance width obtained from the fits might thus be overestimated.

V. CONCLUSIONS

Without any fit of parameters, a microscopic description of the ^{14}O + p elastic scattering provides realistic cross sections. We used two different nucleon-nucleon interactions whose parameters are tuned on the ^{14}C + n mirror system by assuming charge symmetry (the $1/2^+$ and $5/2^+$ experimental energies are employed to constrain the force). The microscopic cross sections obtained with the Minnesota force

are in good agreement with experiment. The Volkov force is known to be more adapted to heavier systems. In this mass region, it overestimates proton widths, and resonant cross sections are therefore in less good agreement with experiment.

A phenomenological R-matrix analysis of recent data [2] is employed to emphasize the different uses of the R matrix and to discuss the validity of the resonance properties. It confirms the properties of the narrow $5/2^+$ resonance but it relies on the sole excitation function at 180°. Other excitation functions might indicate that the width is overestimated. For the broader $1/2^+$ resonance, we suggest a slightly higher energy than in the RGM calculation and than in earlier determinations.

ACKNOWLEDGMENTS

This text presents research results of the Belgian program P5/07 on interuniversity attraction poles initiated by the Belgian-state Federal Services for Scientific, Technical and Cultural Affairs (FSTC). P.D. acknowledges the support of the National Fund for Scientific Research (FNRS), Belgium.

[1] W. A. Peters, T. Baumann, D. Bazin, B. A. Brown, R. R. C. Clement, N. Frank, P. Heckman, B. A. Luther, F. Nunes, J. Seitz, A. Stolz, M. Thoennessen, and E. Tryggestad, Phys. Rev. C **68**, 034607 (2003).

[2] V. Z. Goldberg, G. G. Chubarian, G. Tabacaru, L. Trache, R. E. Tribble, A. Aprahamian, G. V. Rogachev, B. B. Skorodumov, and X. D. Tang, Phys. Rev. C **69**, 031302(R) (2004).

[3] D. Baye, P. Descouvemont, and M. Hesse, Phys. Rev. C **58**, 545 (1998).

[4] K. Wildermuth and Y. C. Tang, in *A Unified Theory of the Nucleus*, edited by K. Wildermuth and P. Kramer (Vieweg, Braunschweig, 1977).

[5] H. Horiuchi, Prog. Theor. Phys. Suppl. **62**, 90 (1977).

[6] Y. C. Tang, in *Topics in Nuclear Physics II*, Lecture Notes in Physics (Springer, Berlin, 1981), Vol. 145, p. 572.

[7] D. Baye and P. Descouvemont, in *Proceedings of 5th International Conference on Clustering Aspects in Nuclear and Subnuclear Systems*, *Kyoto, Japan, 1988*, edited by K. Ikeda, K. Katori, and Y. Suzuki, [J. Phys. Soc. Jpn. Suppl. **58**, 103 (1989)].

[8] A. B. Volkov, Nucl. Phys. **74**, 33 (1965).

[9] Y. C. Tang, M. LeMere, and D. R. Thompson, Phys. Rep. **47**, 167 (1978).

[10] C. Angulo, M. Azzouz, P. Descouvemont, G. Tabacaru, D. Baye, M. Cogneau, M. Couder, T. Davinson, A. Di Pietro, P. Figuera, M. Gaelens, P. Leleux, M. Loiselet, A. Ninane, F. de Oliveira Santos, R. G. Pizzone, G. Ryckewaert, N. de Séréville, and F. Vanderbist, Nucl. Phys. **A716**, 211 (2003).

[11] M. Abramowitz and I. A. Stegun, *Handbook of Mathematical Functions* (Dover, New York, 1970).

[12] D. Baye and N. Pecher, Bull. Cl. Sc. Acad. Roy. Belg. **67**, 835 (1981).

[13] D. Baye and P. Descouvemont, Nucl. Phys. **A407**, 77 (1983).

[14] D. Baye, P.-H. Heenen, and M. Libert-Heinemann, Nucl. Phys. **A291**, 230 (1977).

[15] A. M. Lane and R. G. Thomas, Rev. Mod. Phys. **30**, 257 (1958).

[16] P. Descouvemont and M. Vincke, Phys. Rev. A **42**, 3835 (1990).

[17] R. F. Barrett, B. A. Robson, and W. Tobocman, Rev. Mod. Phys. **55**, 155 (1983).

[18] M. Hesse, J.-M. Sparenberg, F. Van Raemdonck, and D. Baye, Nucl. Phys. **A640**, 37 (1998).